Electrochimica Acta 55 (2010) 8545–8555

Contents lists available at ScienceDirect

Electrochimica Acta

journal homepage: www.elsevier.com/locate/electacta

Diffusion potentials in porous mortar in a moisture state below saturation

Ueli Angst[a,*], Bernhard Elsener[b,c], Roar Myrdal[d], Øystein Vennesland[a]

[a] NTNU Norwegian University of Science and Technology, Department of Structural Engineering, Richard Birkelandsvei 1A, N-7491 Trondheim, Norway
[b] ETH Zurich, Institute for Building Materials (IfB), ETH Hönggerberg, CH-8093 Zurich, Switzerland
[c] University of Cagliari, Department of Inorganic and Analytical Chemistry, I-09142 Monserrato, Cagliari, Italy
[d] SINTEF Building and Infrastructure, N-0314 Oslo, Norway

ARTICLE INFO

Article history:
Received 5 May 2010
Received in revised form 27 July 2010
Accepted 27 July 2010
Available online 6 August 2010

Keywords:
Diffusion potential
Membrane potential
Permselective behaviour
Cement based material
Ion selective electrode

ABSTRACT

Diffusion potentials (membrane potentials) were measured in mortar in a moisture state below saturation for the first time. In contrast to conventional diffusion cell setups, the experimental approach was based on embedded ion selective electrodes. A numerical model with coupled Nernst–Planck equations for the most abundant species in the pore solution allowed simulating ion transport processes and the correspondingly arising diffusion potentials. It was found that Portland cement mortar with a water/cement ratio of 0.6 does not exhibit any significant permselective behaviour – even not in an unsaturated state determined by self-desiccation. Apparently, the stable radius of water-filled capillaries is still large enough to allow ionic transport through those fractions of pore solution that are unaffected by double layer effects. In addition, the relative importance of liquid junction potentials at the reference electrode/sample interface and internal diffusion or membrane potentials are discussed with respect to application of direct potentiometry to cement based materials.

1. Introduction

Diffusion potentials arise from differences in ionic mobility, i.e. differences in velocity of ion movement. In dilute sodium chloride solutions, for instance, chloride has a higher mobility than sodium. Thus, in the presence of a concentration gradient as driving force for diffusion, chloride ions tend to move faster. In order to maintain electroneutrality, however, an electrical field is established that decelerates chloride ions and accelerates sodium ions. This electrochemical potential is called diffusion potential [1].

Several authors have found that within the pore system of hardened cement paste, the diffusivity of halide ions is generally higher than that of alkali ions [2–6] and that the difference in diffusivity increases with decreasing water/cement ratio (w/c) [3], compare Table 1 [2,4–8]. This phenomenon is usually attributed to the electronegative character of cement hydration products and referred to as permselective behaviour of cement paste. A direct consequence of larger differences in ionic mobility is that the above-mentioned diffusion potentials get larger (which, under this effect of permselective properties, are often referred to as *membrane potentials*).

In the presence of differences in ionic concentrations in concrete, e.g. chloride or pH profiles, internal membrane potentials arise. The permselective character of cement paste not only has an effect on ion transport, which was investigated for the specific case of chloride ingress into concrete in various studies [6,9–12], internal membrane potentials also affect any potential measurement through concrete. Particularly for the application of ion selective electrodes as chloride or pH sensors in concrete, diffusion potentials are likely to form a serious error source [13–15].

Attempts to measure membrane potentials in cement based materials have been reported in the literature [6,10–12], where the experimental setup always was of a common diffusion cell type: Cement paste or mortar discs were installed between two compartments containing KCl [10] or NaCl [6] solutions of different concentrations in order to impose a concentration gradient. Occasionally, one compartment contained NaCl and the other an alkaline solution [11,12]. Membrane potentials were measured between reference electrodes placed in the two compartments, eventually taking into account liquid junction potential errors arising at the frit of the reference electrodes. These setups have, however, some disadvantages: First of all, owing to the large differences in chemical composition between the pore liquid inside the specimen and the solutions in the upstream and downstream compartments, diffusion potentials are established at the specimen/solution interfaces (in addition to the internal membrane potential). Especially in the case of exposure to neutral salt solutions in the compartments, the large pH difference causes significant diffusion potentials. As only the sum of all diffusion potentials present between the reference electrodes can be measured, the interfacial potential drop might overshadow internal membrane potentials arising from the globally imposed concentration gradient of e.g. sodium chloride. In addition, ions are leached out of the specimen and change the

* Corresponding author. Tel.: +47 735 94 538.
E-mail address: ueli.angst@ntnu.no (U. Angst).

0013-4686/$ – see front matter © 2010 Elsevier Ltd. All rights reserved.
doi:10.1016/j.electacta.2010.07.085

Table 1
Intrinsic diffusion coefficients in cement paste and mortar (measured at saturation) and diffusion coefficients for dilute bulk solutions at ambient conditions.

Ref.	w/c	Diffusion coefficients (10^{-12} m^2/s)				Ratios		Remarks on experimental setup
		Chloride	Hydroxide	Sodium	Potassium	D_{OH^-}/D_{Cl^-}	D_{Cl^-}/D_{Na^+}	
Goto and Roy [2]	0.35	–		0.41			–	Portland cement paste discs (0.3 cm thick, 4 weeks old, cured in sat. $Ca(OH)_2$) mounted in diffusion cell setup between deionised water and 0.5 M NaCl
	0.4	6.9		1.46			5	
	0.45	7.5		0.84			9	
Tuutti [7]	0.4	0.8–5	6–10			2–7.5		Mortar samples (OPC, ca. 1 year old), one side exposed to 3% NaCl solution; D calculated from free Cl^- and OH^- concentrations in expressed pore solution
	0.6	4–12	10–30			ca. 2.5		
Chatterji and Kawamura [4]	0.4	8.2		1.4			6	Portland cement paste discs (7-d old, water cured) mounted in diffusion cell setup between dist. water and 1 M NaCl
Chatterji [5]	0.4	1.8–3.2		0.19–0.33	–		5–17	Low alkali, low C_3A cement paste discs (3 mm thick, 7-d old, water cured) mounted in diffusion cell setup between dist. water and various salt solutions
		1.9–3.7		–	0.2–0.46			
Elakneswaran et al. [6]	0.4	ca. 4.2		ca. 1.0			4	Portland cement paste discs (5 mm thick, 28-d old, cured in sat. $Ca(OH)_2$) mounted in diffusion cell setup between various NaCl solutions
	0.5	8.7		ca. 1.5			6	
	0.6	16.1		ca. 2.5			6	
Handbook of Chemistry and Physics [8]		2.03×10^3	5.27×10^3	1.33×10^3	1.96×10^3	2.6	1.5	Tabulated data valid for dilute bulk solutions

magnitude of interfacial diffusion potentials over time. Another drawback of diffusion cell arrangements is that mortar or cement paste specimens are in a saturated state. In practice, on the other hand, concrete is generally unsaturated. Since the diffusivity decreases with a reduction in water content [16], experimental results from saturated specimens are not applicable to the realistic case of concrete below saturation.

The present study aims at measuring membrane potentials in self-desiccated and thus unsaturated mortar. The experimental setup is based on embedded ion selective electrodes (ISE) rather than on a diffusion cell arrangement. This allows measurement below saturation as well as avoiding the experimental difficulties imposed by the presence of sample/external solution interfaces. In the first part of the paper, the experimental setup is presented, followed by measurement results. The sample is characterised by numerous parameters in order to provide a useful basis for the discussion that includes a numerical model for the internal membrane potential based on Nernst–Planck equations. Special attention is paid to separating the effects of interfacial liquid junction and internal membrane potentials.

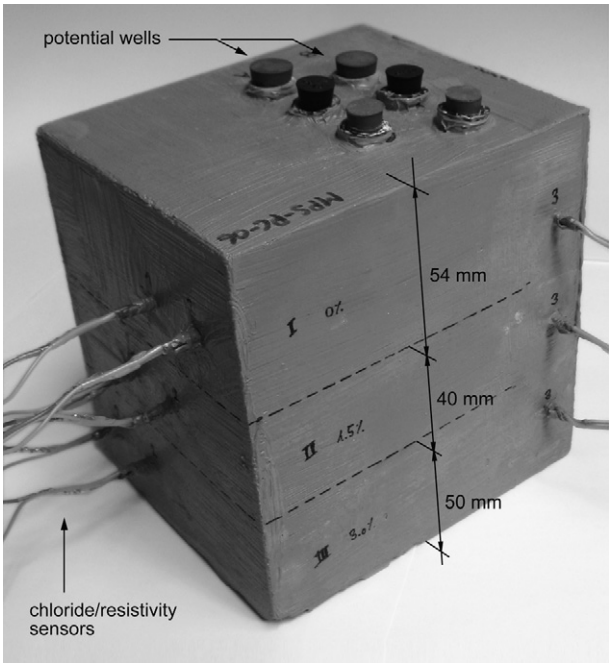

Fig. 1. Sample (120 mm × 140 mm × 144 mm), with 9 embedded chloride/resistivity sensors sticking out. The mortar layers I–III can be accessed with external reference electrodes through two potential wells each.

2. Experimental

2.1. Sample specifications

A mortar sample was cast consisting of three layers of mortar with different contents of mixed-in sodium chloride. Each layer was poured into the mould ca. 2 h after the previous one (wet-on-wet casting). The sample geometry is shown in Fig. 1 and the mix proportions are given in Table 2. The mortar was mixed in a laboratory planetary mixer (Hobart A200) following the standard procedure of our laboratory (1 min dry mixing, 2 min wet mixing, 2 min resting, 1 min mixing on second speed). Three ion selective electrodes (ISEs) were embedded in each of the layers (9 ISEs in total), enabling thus to get an average or multiple single measurement values. It is suggested that this is equal to an approach with several parallel samples. The ion selective electrodes exhibit an electrochemical potential depending on the chloride ion activity in the pore solution of the respective mortar layer. In addition, as the ISEs were mounted in stainless steel tubes, the electric resistance between two tubes could also be measured; details about these sensors are reported elsewhere [15,17].

Cylindrical PTFE-bars were fixed in the formwork before casting and drawn out of the hardened mortar at the time of demoulding

Table 2
Mix proportions (by weight) for the three layers (batch size per mix = 6.1 kg).

	Mix I	Mix II	Mix III
Portland cement (CEM I 52.5 N)	1	1	1
Sand 0–2 mm (filler content 24%)	3	3	3
Water	0.6	0.6	0.6
Chloride by weight of cement	–	1.5%	3.0%

(1 d after casting). A plastic hose was immediately glued into the hole, thereby sealing the lateral mortar surface of the hole, and closed with a rubber plug on the top side. These "potential wells" allow placing an external reference electrode in the hole and thus at the same depth as the ISEs. In the present work saturated calomel electrodes (SCEs) were used as reference electrodes. By placing two SCEs in two different potential wells it was possible to measure the sum of liquid junction and membrane potentials between the two reference electrodes. In addition, the potentials of the ISEs could be measured vs. differently located reference electrodes by using different potential wells. In order to establish electric contact between the frit of the reference electrode and the mortar, a small piece of textile material was placed on the bottom of each potential well and wetted with a droplet of electrolyte solution (the chemical composition of the used electrolytes is given in Section 3 when presenting the respective results).

After demoulding, all outer sample surfaces were painted with an epoxy based resin to avoid exchange of moisture with the environment. The achieved internal moisture state was thus determined by self-desiccation (i.e. the internal moisture equates entirely to the water not consumed in the hydration reaction of cement and water). The temperature was constantly around 20–22 °C during all the experiments.

2.2. Measurements

Potentials of the ISEs and electric resistances (AC, f = 1 kHz) were recorded over time as described above. To transform the measured resistance into resistivity, conversion factors were calculated by use of the finite-element program COMSOL Multiphysics [18] for the various relative geometrical arrangements of the steel tubes. One of these cell constants was checked experimentally by measuring the resistance between two tubes fixed in the mould, which was filled with a solution of known conductivity.

After more than 2 months, 15–20 mm thick plates were cut from part of the mortar sample, broken into pieces and immediately subjected to pore solution expression. From the remaining part of the sample, mortar layers of ca. 3–4 mm thickness were cut by use of a dry saw in order to determine the internal profile of total chloride. All the taken samples were powdered and the acid-soluble chloride content analysed (extraction procedure: 6.5% nitric acid, 30 s stirring at 80 °C, dissolution time 1–3 h at ambient temperature; chloride analysis by a spectrophotometric method).

At the time of casting, 10–12 plastic bottles (100 ml volume) were filled with mortar from each mix, sealed with a screw cap and kept at 20 °C until needed. At specific points in time, the bottles were opened and the mortar used for pore solution expression, acid-soluble chloride analysis and determination of evaporable and nonevaporable water contents.

2.2.1. Pore solution expression

A device as the one described in [19] was used for expressing pore solution from the cylindrical mortar samples. A maximal pressure of 280 MPa was applied and owing to the rather high cement content and high w/c ratio, usually sufficient pore solution was obtained after 20–30 min (up to 6 ml). The solution was kept in sealed vials until chemical analysis. The remaining air in the vials was replaced with a mixture of nitrogen and oxygen to avoid carbonation in the storage period. The solution was analysed for hydroxide ion concentration by potentiometric titration and chloride by chromatography. In some selected samples, also potassium, sodium, calcium, aluminium, iron and sulphate ion concentrations were analysed.

2.2.2. Evaporable and nonevaporable water

A mortar sample of at least 30 g was broken into pieces of 2–5 g and dried at 105 °C during ca. 4 h. It was found in preliminary tests that the weight approached a stable value after 3–4 h of drying with a further weight loss of less than 0.5‰ per hour. The upper size limit of 5 g was chosen in order to achieve optimal drying and ignition times, and the lower limit of 2 g was selected in order to minimise carbonation during drying [20]. The weight loss during drying was considered as the evaporable water content, w_{ev}. Subsequently, the sample was ignited at 1000 °C and the nonevaporable water content, w_n, was defined as the mass loss between 105 and 1000 °C divided by the mass of ignited cement. Corrections were made with regard to loss on ignition (LOI) of unhydrated cement (2.1%) and aggregates (0.7%) as determined from separate LOI measurements. To estimate the degree of hydration, it was assumed that the amount of chemically bound water in fully hydrated cement is 0.24 g/g_{cem} [21].

2.2.3. Degree of capillary saturation (DCS)

To estimate DCS, the paste porosity is needed. This can be calculated by applying Power's model, based on his classic work [21,22], in the following form:

$$\varepsilon_p = \frac{\mathrm{w/c} - (1 - 0.254)w_n}{(1/\rho_{cem}) + \mathrm{w/c}} \quad (1)$$

where ρ_{cem} is the density of cement (3.12 kg/dm^3), ε_p is the paste porosity (as volume fraction) and w/c is the water/cement ratio in the mix. DCS was then estimated as follows:

$$\mathrm{DCS} = \frac{w_{ev}}{(1/\rho_{cem}) + \mathrm{w/c}} \frac{1}{\varepsilon_p} \quad (2)$$

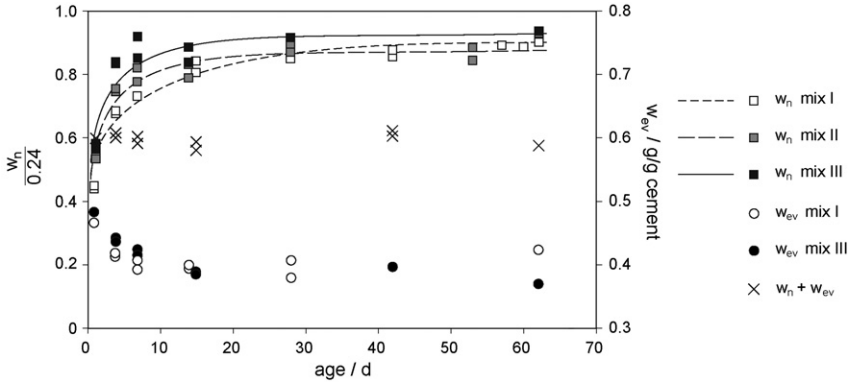

Fig. 2. Evaporable (w_{ev}) and nonevaporable water (w_n) measured on parallel samples. The estimated degree of hydration is plotted vs. the left ordinate; w_{ev} and the sum $w_{ev} + w_n$ are plotted vs. the right ordinate.

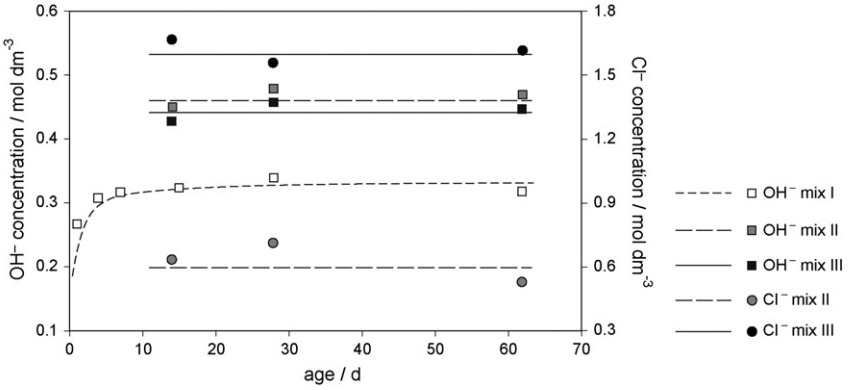

Fig. 3. Hydroxide and chloride ion concentrations in mixes I–III vs. time. Measured on expressed pore solution of separately cured parallel samples.

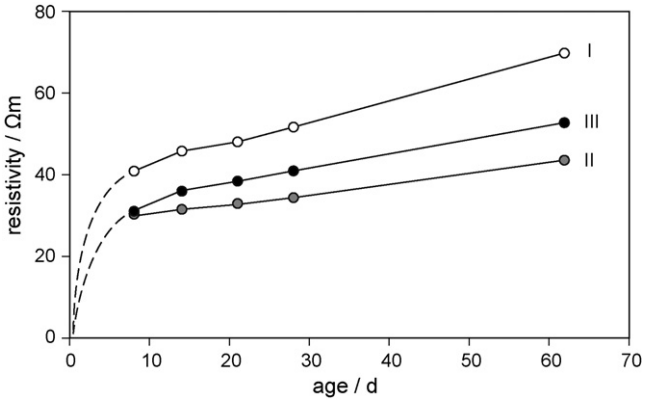

Fig. 4. Electric resistivity vs. time (average of three values per layer).

3. Results

3.1. Process of hydration and pore solution composition

The process of hydration can be followed by examining the chemical and physical parameters displayed in Figs. 2–5 over time. The estimated degree of hydration increases fast and is above 80% by 28 d for all three mixes; thereafter, it only increases slowly. The evaporable water content, on the other hand, decreases in accordance with the evolution of w_n as water is consumed by the hydration reactions. Fig. 2 also clearly illustrates the accelerating effect of chloride. It is interesting to note that the sum of w_n and w_{ev}, both related to cement weight, is close to the theoretical value of 0.6 at all times, which indicates a good accuracy of the measurements.

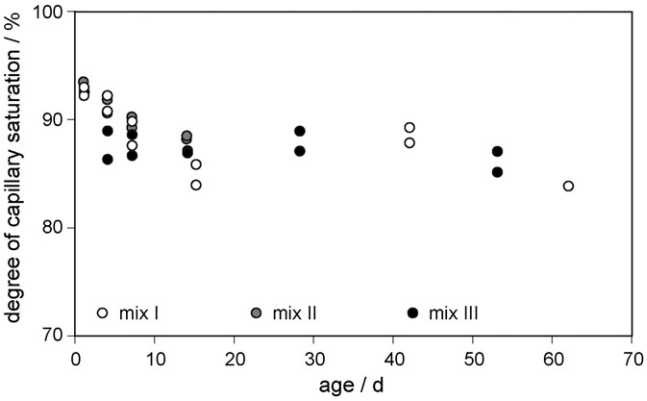

Fig. 5. Estimated degree of capillary saturation as a function of hydration time.

The hydroxide ion concentration in the pore solution follows a similar curve as the one for w_n, but flattens out earlier. In the absence of mixed-in chloride, the stable hydroxide concentration is around 0.32 mol dm^{-3}; in the case of admixed chloride, higher concentrations in the range of 0.43–0.48 mol dm^{-3} are reached. The higher pH in the presence of NaCl can be ascribed to the higher degree of hydration, but might also partly arise from formation of Friedel's salt and the associated release of NaOH when the cation of the chloride salt is sodium [23]. Similar to the hydroxide concentrations, also the chloride concentrations in the expressed pore solution are on stable levels after 15 d, which suggests that any mechanisms involved in chloride binding are at equilibrium. Table 3 shows the results of chemical analysis of pore solution expressed from mix I.

Fig. 4 shows that the electric resistivity of the mortar in the three layers increases almost linearly with time after the age of ca. 15 d. Before that, it must have increased much faster. The resistivity data mirrors the time evolution depicted in Fig. 2 and is in agreement with results reported in the literature [24]. According to Fig. 5, the estimated DCS is in the same range in all three layers. Thus, owing to the absence of gradients in moisture content, there is no internal movement of moisture as an additional mechanism contributing to the transport of ionic species within concrete (in addition to diffusion and migration).

3.2. Potential measurements

Fig. 6 shows the measured potentials of a selected ISE vs. time. It is striking that the potentials are always higher when measured against the SCE placed in layer I compared with the SCE located in layer II or III. Clearly, in the presence of concentration gradients

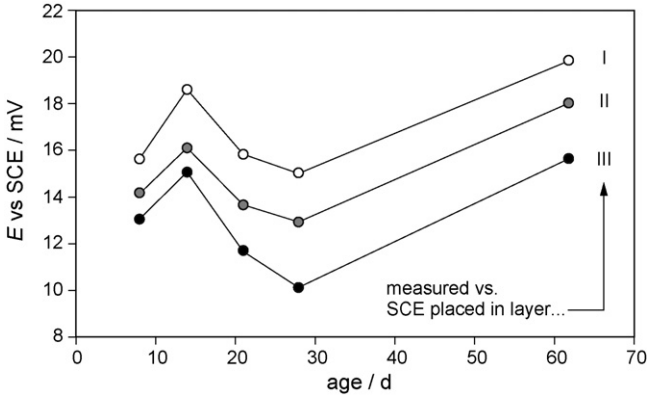

Fig. 6. Measured potentials of an ISE in layer II vs. time. The SCE was placed in potential wells located in different layers with 0.35 M KOH as wetting electrolyte.

Table 3
Composition of pore solution expressed from mix I at the age of 28 d.

	OH^-	Na^+	K^+	Ca^{2+}	Cl^-	Fe^{2+}	Al^{3+}	SO_4^{2-}	$\sum c_{\text{cation}\,i} \cdot z_i$	$\sum c_{\text{anion}\,i} \cdot z_i$
mg/l		4700	6430	81	58	0.26	3.6	240		
mmol dm^{-3}	335	204	164	2.021	1.636	0.005	0.133	2.498	373	−342

$c_{\text{cation}\,i}$ is the concentration of cation i, $c_{\text{anion}\,i}$ the concentration of anion i, and z_i the respective charge number.

in the concrete, the location of the reference electrode is important. Similar graphs were obtained for the other ISEs, whereas some are up-and-down-shaped as the one in Fig. 6 and others follow monotonously increasing or decreasing curves. Measurement vs. an SCE placed in layer I always gave higher potentials and the curves were in all cases almost parallel. There are several possible reasons for the instability of the ISE potentials: The chloride ion activity at the sensor might be affected by (1) chloride binding, (2) diffusion or other transport processes, and (3) release of hydroxide ions during hydration. Moreover, liquid junction potentials at the SCE/concrete interface might also be inconstant over time since the mortar exposed in the potential well is diluted with wetting electrolyte every time a measurement is conducted. The fluctuations in recorded potentials are, however, in the range of only a few mV (Fig. 6).

It was in a previous publication [14] observed that the composition of the contacting electrolyte is a decisive parameter for the measurement of ISE potentials. One might thus consider that the pore solution at the concrete surface inside the potential wells might have changed over time (due to contact with 0.35 M KOH and KCl from the SCE, as well as CO_2), and thereby give rise to diffusion potential errors. To avoid these uncertainties, holes were drilled from the lateral sample side to expose pristine concrete (at a sample age of 72 d). The holes were located at the same depth as the embedded ISEs. In order to minimise the liquid junction potential at the SCE/concrete interface, pore solution – obtained from pore solution expression – was used as wetting electrolyte: solution expressed from mix I (separately cured samples) was used for the SCE placed in holes in layer I, solution from mix II to establish contact in layer II, etc. For reason of comparison, the same measurements were carried out with 0.35 M KOH as contacting electrolyte in additional unspoilt concrete holes (at the same depth). The results are depicted in Fig. 7, clearly showing the effect of different wetting electrolytes. The influence is more pronounced for junctions in layer II and III because the difference in composition between pore solution and used wetting electrolyte is larger: The hydroxide ion concentration in layer I is close to 0.32 mol dm^{-3} (Fig. 3) and thus the expressed pore solution used in this layer is similar to 0.35 M KOH.

If the potential of a certain ISE is measured vs. SCEs placed in different layers, the recorded value consists of several contributions. This is schematically depicted in Fig. 8. In the first case, the ISE potential, E_{ISE}, is measured vs. an SCE placed in the same layer (II). There is a liquid junction potential, E_{j1}^{II}, between the internal reference electrode solution (sat. KCl) and the wetting electrolyte, as well as a liquid junction potential, E_{j2}^{II}, at the interface wetting electrolyte/concrete pore solution in layer II. In the case of an SCE placed in layer I (case b), an additional contribution adds to the measured potential, namely the membrane potential arising from internal concentration differences between layer I and II, $E_{\varphi}^{\text{I–II}}$. For these two cases, the measured ISE potential, E_m, can be written as follows:

$$\text{Case a:} \quad E_m^a = E_{ISE} - E_{SCE} + E_{j1}^{\text{II}} + E_{j2}^{\text{II}} \tag{3}$$

$$\text{Case b:} \quad E_m^b = E_{ISE} - E_{SCE} + E_{j1}^{\text{I}} + E_{j2}^{\text{I}} + E_{\varphi}^{\text{I–II}} \tag{4}$$

When the respective expressed pore solutions were used as wetting electrolyte, E_{j2}^{I} and E_{j2}^{II} are close to zero since the composition of wetting electrolyte and internal pore solution is very similar.

Subtracting Eq. (4) from Eq. (3) and solving for $E_{\varphi}^{\text{I–II}}$ yields:

$$E_{\varphi}^{\text{I–II}} = \Delta E_m^{b-a} - E_{j1}^{\text{I}} + E_{j1}^{\text{II}} \tag{5}$$

The liquid junctions E_{j1}^{I} and E_{j1}^{II} can be calculated by the Henderson equation (assuming the absence of membrane behaviour, which is essentially true), and thus, it is possible to calculate the membrane potential, $E_{\varphi}^{\text{I–II}}$. In an analogous manner, the membrane potentials between the other layers can be calculated as well.

For the sake of completeness, it should be mentioned that the composition of the pore solutions expressed from separately cured parallel samples, which was here used as wetting electrolyte, is not

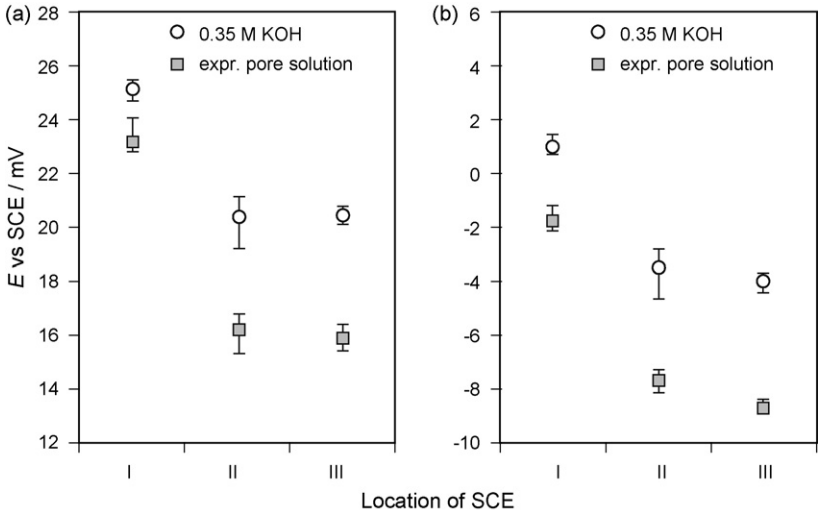

Fig. 7. Potentials of two selected ISEs measured vs. SCE placed on freshly exposed concrete in different layers I–III as well as with two different wetting electrolytes. Average and max/min values based on measurements in three freshly drilled holes per type of wetting electrolyte and two measurements in each hole. (a) Shows an ISE embedded in layer II and (b) an ISE in layer III.

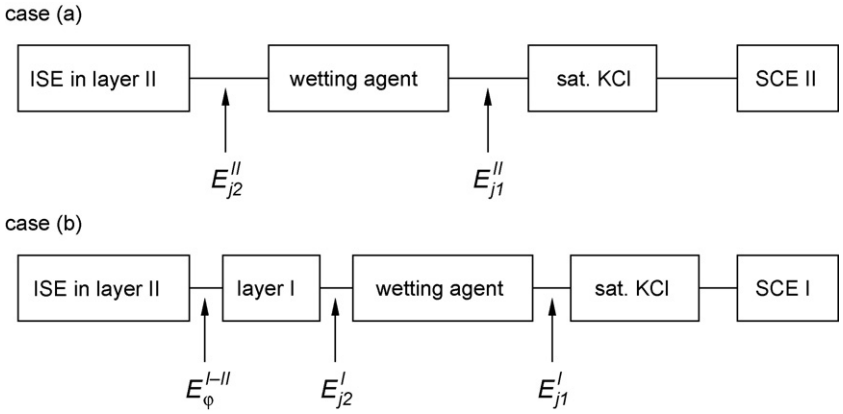

Fig. 8. Contributions to diffusion potentials when measuring vs. two SCEs placed in different potential wells.

identical with the solution actually present inside the mortar at the time of measurement. The reasons for deviations are diffusion inside the mortar sample containing three layers of different mixes (as will be shown later) or effects of the pore solution expression technique such as the high pressure and increase in temperature during expression that might affect the equilibrium between solid and dissolved species in the paste. It is thus likely that small diffusion potentials also arise at the interface of wetting electrolyte and internal pore solution. However, when subtracting Eq. (4) from Eq. (3) it would be the difference of E_{j2}^{I} and E_{j2}^{II} that induces such an error. While the absolute values of E_{j2}^{I} and E_{j2}^{II} might differ slightly from zero, the difference is likely to become negligible.

Membrane potentials calculated in an analogous manner to Eq. (5) are shown in Fig. 9 (circles). In addition, membrane potentials measured directly between two SCEs inserted in potential wells in different mortar layers are depicted as square symbols (corrected for liquid junction potentials in the same way as the measurements described above). As apparent from the graph, the membrane potentials obtained by these two different ways are in good agreement.

According to Fig. 9, membrane potentials between layers II and III are small, viz. in the range ±2 mV. This is in agreement with theoretical estimations made in an earlier publication by two of the present authors [14], where it was shown that diffusion potentials arising from a difference in chloride concentration are only a few mV as long as the pH is higher than 13.5. According to the data given in Fig. 3, the pH is around 13.65 in layers II and III, and the difference in chloride concentration is rather large (around 1 mol dm^{-3}). Still, the membrane potential is of insignificant magnitude. When

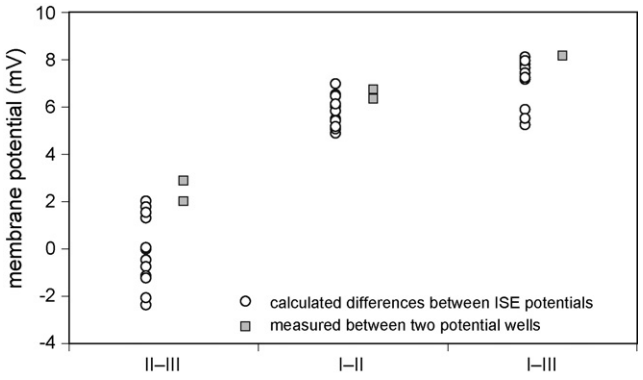

Fig. 9. Observed membrane potentials between different mortar layers (using the respective expressed pore solution as wetting electrolyte; measurements corrected for liquid junction potentials).

internal gradients in pH are present, it was in Ref. [14] estimated that diffusion potentials can easily reach 5–10 mV even for a difference in pH as small as 0.2 units. In the present case, ΔpH between layers I and II or layers I and III are ca. 0.15 units and the experimentally determined membrane potentials are in the estimated range mentioned above. It is noticeable that the observed membrane potentials are similar despite the clearly different chloride concentration gradients between layers I and II ($\Delta c(Cl^-) \approx 0.6$ mol dm^{-3}) and layers I and III ($\Delta c(Cl^-) \approx 1.6$ mol dm^{-3}). The difference in pH overshadows any effects arising from chloride concentration gradients.

3.3. Chloride contents

Fig. 10a shows the chloride content determined as acid-soluble chlorides on mortar discs cut from the sample at the age of more than 2 months. In addition, the initial chloride content is plotted for each layer: the known amount of admixed chloride (long dashed line) as well as the one determined as acid-soluble chlorides from parallel samples cast from the same batch (short dashed line). This data shows that the used procedure for measuring acid-soluble chlorides is not capable of finding the true total chloride content. It was mentioned by Dhir et al. [25] that only part of the total chlorides are dissolved in common acid extraction techniques. In the present study, the detected acid-soluble chloride content is in the range 65–90% of the amount of true (admixed) chloride. The final analyses of acid-soluble chlorides at different depths of the mortar sample plotted in Fig. 10a show that diffusion has lead to a gradual chloride profile a little more than 2 months after casting. At the depth of sensor in layer I, the chloride content has increased to ca. 0.25% per cement weight. At the sensors in layer III, on the other hand, the total chloride content appears to be in the same range as the initial value, perhaps slightly lower. The individual values found from different discs scatter noticeably, the differences at the same depth being up to 0.5% chloride by cement weight. This variability might be result from inhomogeneous chloride distributions as well as from uncertainties associated with the procedure to determine the total chloride content.

Corresponding free chloride concentrations are depicted in Fig. 10b. Both the values obtained from pore solution of 15–20 mm thick discs cut from the mortar sample and the concentrations measured by means of the embedded ion selective electrodes gave similar results. For the latter, potentials measured with expressed pore solution as wetting electrolyte were used and transformed into chloride concentration according to a procedure described elsewhere [15]. Fig. 10 also shows that the values from pore solution expression of discs and those potentiometrically obtained are somewhat lower than the values obtained from pore solu-

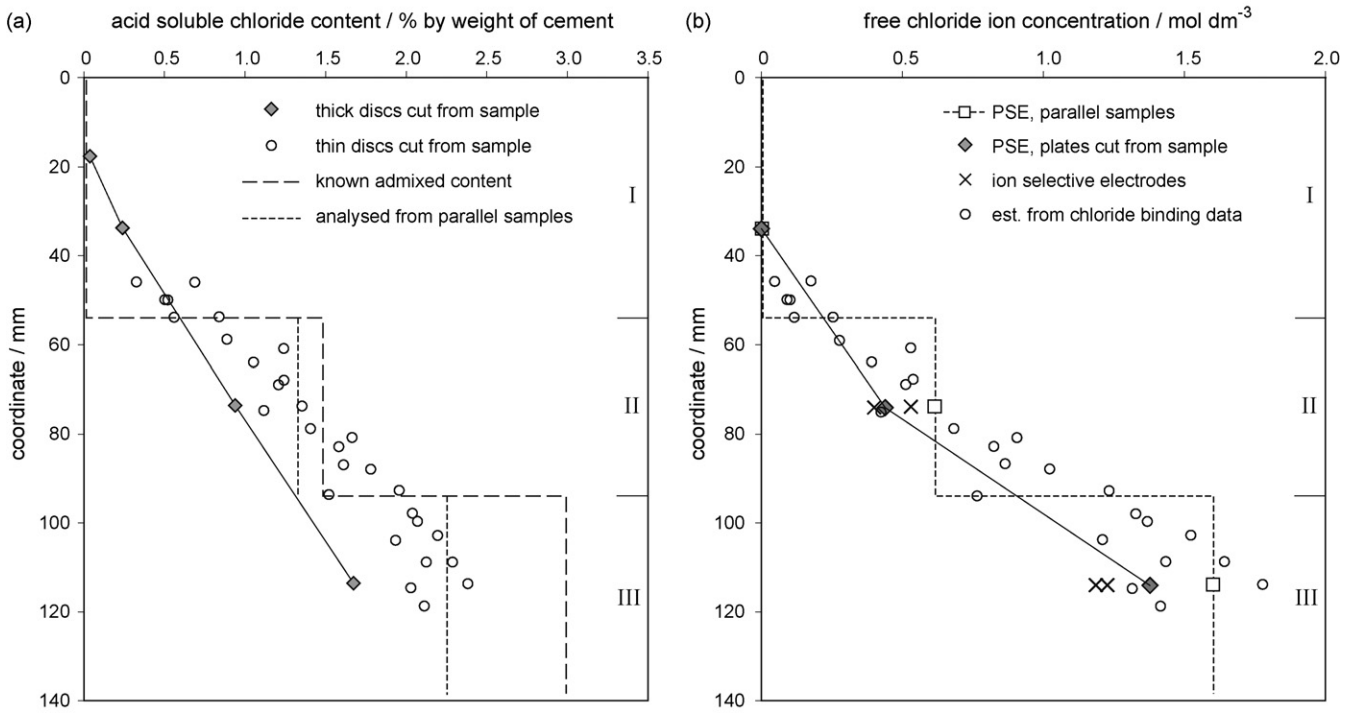

Fig. 10. Total and free chloride contents at different depths.

tion expression of parallel samples (stored in bottles) from the respective mortar mixes. By the use of chloride binding data, the free chloride concentrations corresponding to the total chloride contents of the thin discs (Fig. 10a) can be estimated. Such an estimation was based on chloride binding data from Ref. [15] as well as from the present study and the results are also plotted in Fig. 10b. The overall data of free chloride concentrations reflects the trend shown in Fig. 10a, that is the elimination of the initially steplike chloride distribution in the mortar sample.

Table 4 shows the ion concentrations at the depth of the sensors at the time of cutting discs from the mortar sample. The pore solution composition in layer I is very similar to the one measured on a parallel sample at the age of 28 d (Table 3). This indicates that internal diffusion of hydroxide and other ions has not yet reached the depth of the sensor in this layer. In the case of layers II and III, on the other hand, chloride and hydroxide concentrations are lower than in the samples separately cured in the absence of concentration gradients as driving force for diffusion (Fig. 3).

4. Numerical model

4.1. Equations and parameters

The well-known Nernst–Planck equation describes the total ionic flux under the simultaneous effects of a concentration gradient (chemical potential) and an electric field (such as diffusion potentials) [1]. For the case of one-dimensional ionic transport it can be written in the following, differential form (by including an additional advection term):

$$\frac{\partial c_i}{\partial t} = \frac{\partial}{\partial x}(J_{diff} + J_{mig} + J_{adv}) = \frac{\partial}{\partial x}\left(D_i \frac{\partial c_i}{\partial x} + D_i c_i \frac{z_i F}{RT}\frac{\partial \phi}{\partial x} - c_i v_x\right) \quad (6)$$

In this equation, c_i is the concentration (mol/m^3) and J_{diff}, J_{mig} and J_{adv} denote the fluxes (mol m^{-2} s^{-1}) owing to diffusion, migration and advection, respectively. D_i is the diffusion coefficient (m^2/s) and z_i the charge number of ion i. F refers to Faraday constant (96,485 C/mol), R to the gas constant (8.314 J mol^{-1} K^{-1}), T is the temperature (K) and the electric potential is denoted ϕ (V). The last term represents the transport by advection, where v_x is the velocity of the fluid in x direction (m/s).

To model ionic transport, Nernst–Planck equations have to be set up for every involved charged species and solved simultaneously. The unknowns for a certain point in time and space are the electric potential, ϕ, and the concentrations of all the involved ions, c_i. The set of equations is solvable since the ionic concentrations are coupled through the electroneutrality condition, which states that the net charge must at all times vanish in every control volume:

$$\sum z_i \cdot c_i = 0 \quad (7)$$

The finite-element software COMSOL Multiphysics [18] offers a module for modelling transport of charged species in this way. For the present case, a one-dimensional model was selected in order to simulate ionic transport between the three layers. Since Fig. 5 indicates that there is no internal moisture redistribution, the advection term in Eq. (6) was omitted: $v_x = 0$.

Nernst–Planck equations were set up for chloride, hydroxide, potassium and sodium ions as these are the most abundant species in the pore solutions (Tables 3 and 4). Moreover, these are the most mobile ions; calcium ions, which are also present in hardened cement paste, are much more strongly adsorbed to electronegative hydration products owing to the higher charge number [5]. The mass balance equations of each ionic species, solved by the software, are identical to Eq. (6). For the first species (in the present

Table 4
Ion concentrations (mol dm^{-3}) obtained from pore solution expression of 15–20 mm thick mortar discs cut from the depth of embedded ion selective electrodes (at age = 72 d).

	OH^-	Cl^-	Na^+	K^+
Layer I	0.328	0.004	0.209	0.166
Layer II	0.417	0.426	0.653	0.151
Layer III	0.421	1.376	1.522	0.192

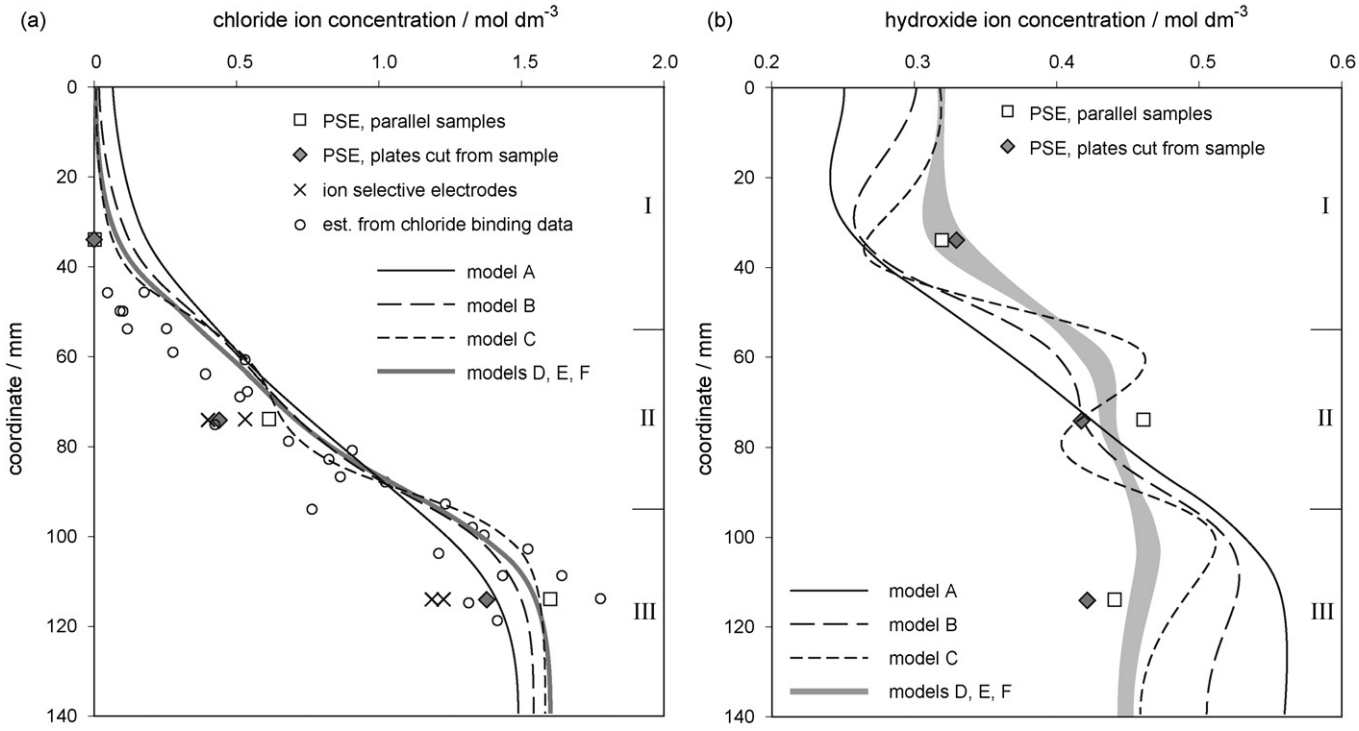

Fig. 11. Experimentally determined and modelled chloride and hydroxide ion concentrations in the pore solution at age = 72 d.

Table 5
Initial ion concentrations (10^3 mol m^{-3}) in the three layers for the numerical models (based on pore solution expression from parallel samples).

	OH^-	Cl^-	Na^+	K^+
Layer I	0.32	0.002	0.179	0.143
Layer II	0.46	0.6	0.59	0.47
Layer III	0.44	1.6	1.13	0.91

model sodium was arbitrarily selected), the mass balance equation is replaced by the following one, which evolves from combining the mass balance equations written for all the involved ionic species, i.e. for sodium, chloride, hydroxide and potassium, and the electroneutrality condition (Eq. (7)):

$$\frac{\partial}{\partial x}\left(\sum z_i\left(D_i\frac{\partial c_i}{\partial x}+D_i c_i\frac{z_i F}{RT}\frac{\partial \phi}{\partial x}\right)\right)=0 \quad (8)$$

The parameters for the models, that is the initial concentration in the three layers and the sets of studied diffusion coefficients, are summarised in Tables 5 and 6. For models A–C, pronounced differences between the diffusivities of cations and anions were selected in order to simulate a strong permselective effect of the cement paste; for these cases, the ratios D_{Cl^-}/D_{Na^+} and D_{OH^-}/D_{Cl^-} were selected according to Refs. [12,14]. The ratios in model F are identical or close to values for dilute bulk solutions (i.e. it simulates the absence of permselective behaviour). Parameters in model D were selected to simulate the case of significantly higher hydroxide ion diffusivity compared with chloride, sodium and potassium; model E was selected to study the case of D_{OH^-}/D_{Cl^-} as in bulk solution, but with a slightly elevated chloride diffusivity with respect to cations. The simulations were run in a time-dependent mode until t = 72 d.

Table 6
Diffusion coefficients used in the numerical model.

	Model					
	A	B	C	D	E	F
D_{Cl^-} (10^{-11} m^2/s)	10	5	2	2	2	2
D_{OH^-} (10^{-10} m^2/s)	7.5	3.8	1.5	1.5	0.5	0.5
$D_{Na^+} = D_{K^+}$ (10^{-12} m^2/s)	13.3	6.7	2.7	10	8	13.3
D_{Cl^-}/D_{Na^+}	7.5	7.5	7.5	2	2.5	1.5
D_{OH^-}/D_{Cl^-}	7.5	7.5	7.5	7.5	2.6	2.6

Although, the Nernst–Planck equation describes mass transport in dilute solutions and is principally not valid for concentrated solutions owing to short-range interactions between ions, it has several times been successfully used as a basis for modelling ionic transport in cementitious systems, e.g. Ref. [26]. The diffusion coefficients as input parameters for the model are strictly speaking required to be self-diffusion coefficients, which are, however hard to measure experimentally. The literature values summarised for cement paste and mortar in Table 1 are all intrinsic diffusion coefficients determined with procedures that always also include some effects of all the other ions present in the mass transport. They are, however, considered as a reasonable starting point for an estimation of the individual self-diffusion coefficients assumed in Table 6. Note that the present model does also not take into account that during the course of hydration, diffusivities are decreasing owing to first concrete setting and the later increase in pore tortuosity. The selected diffusion coefficients are considered as average values over time and are thus slightly higher than what was found in Ref. [6] for 28-d old cement paste for the same water cement ratio (Table 1). Also time-dependent changes in pore solution composition owing to release of ions from hydration reactions as well as binding reactions were neglected in the present model.

4.2. Results

Chloride and hydroxide ion concentration profiles calculated from the numerical models are compared with experimental values in Fig. 11. The effect of model parameters on free chloride profiles after 72 d is relatively small when compared with the scatter of the experimentally obtained values. Considering the low chloride concentrations measured in layer I, the diffusivities selected in models C–F gives the most reasonable results.

Fig. 11 illustrates the effect of diffusion potentials on ionic transport: owing to the pronounced chloride concentration gradient, a strong driving force for chloride diffusion is present in the sample. The higher the chloride diffusivity, the more chloride ions move towards layer I (illustrated by models A–C). In order to satisfy electroneutrality, either must cations co-diffuse with chloride ions or hydroxide ions must move in the opposite direction. When the diffusivity of cations is much lower than that of anions, which is the case in models A–C ($D_{Cl^-}/D_{Na^+} = 7.5$), movement of hydroxide is the favoured process to maintain charge balance. This actually decreases the hydroxide concentration in layer I and increases it in layer III (Fig. 11b), even though the driving force for pure diffusion of hydroxide is opposite. In this case, the second term in Eq. (6) is larger than the first one that describes the diffusion flux and thus migration dominates the transport of hydroxide ions. Measurements have, however, shown that the pH did not change much in the three layers. This implies that the differences between anion and cation diffusivity cannot be that large. Accordingly, models D–F show better agreement with experimental data. The effect of hydroxide movement to maintain electroneutrality was also experimentally observed by other researchers in Ref. [27].

Fig. 12 shows the modelled membrane potentials after 72 d. The magnitude of membrane potentials depends on (1) concentration gradients of the involved species, and (2) ratios of ionic mobility (or diffusivity) of cations and anions. When the latter are kept constant (models A–C), it is the hydroxide concentration differences reached by that time that determine the established membrane potentials. The shapes of the three curves A–C in Fig. 11b are clearly reflected by those in Fig. 12; the more pronounced the hydroxide concentration differences, the larger the membrane potentials. When, on the other hand, the concentration profiles are similar such as in models D–F (Fig. 11), it is the ratio of ion diffusivities that solely governs the magnitude of membrane potentials. The closer these ratios are to the values in dilute bulk solutions (model F), especially the ratio of cation and anion mobility, the smaller is the membrane potential. Comparison with the experimental data depicted in Fig. 9 shows that model F agrees best: the largest part of membrane potential is established between layers I–II and I–III (where there are strong gradients in chloride and hydroxide concentrations); the membrane potentials between layers II and III is negligible (owing to the low hydroxide gradient and generally high pH).

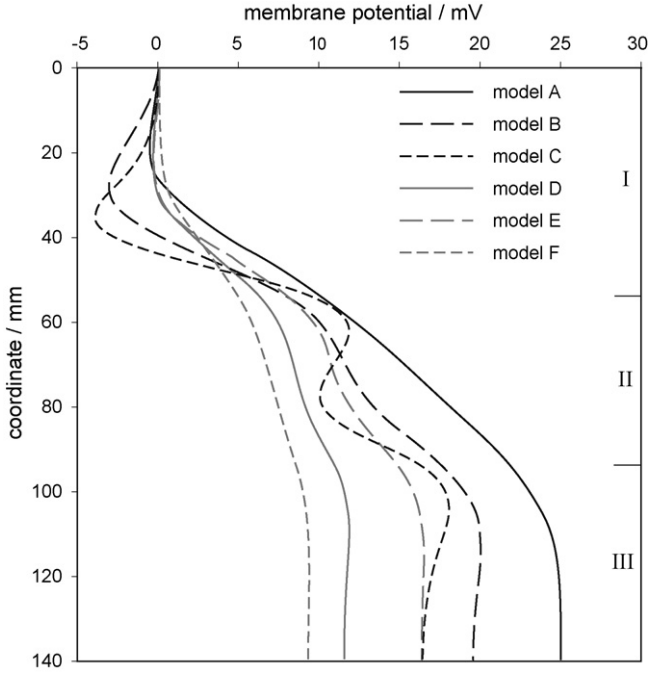

Fig. 12. Modelled membrane potentials at age = 72 d.

5. Discussion

5.1. Membrane behaviour of porous mortar

In mortar with w/c = 0.6 and a moisture state below saturation (resulting from self-desiccation), diffusion potentials can successfully be simulated by use of a numerical model based on coupled Nernst–Planck equations. The diffusion coefficients (averaged over time) that yield good agreement with experimental data are as follows: $D_{Cl^-} \approx 2 \times 10^{-11}$ m^2/s, $D_{OH^-} \approx 5.2 \times 10^{-11}$ m^2/s, and $D_{Na^+} = D_{K^+} \approx 1.3 \times 10^{-11}$ m^2/s. These diffusivities are by two orders of magnitude lower than in dilute bulk solutions (Table 1), which is a consequence of the tortuosity and constrictivity of diffusion paths (pores) [3] and the high ionic strength (ion interactions). The ratios between ionic mobilities, on the other hand, are close to the values for dilute bulk solutions. This implies that the present mortar does not behave like a permselective membrane, i.e. it does not significantly retain movement of specific ions such as cations.

Owing to the negative charge of hydrated cement particles, positive ions are adsorbed in the double layer, whereas negative ions are more concentrated in those parts of pore solution farther away from pore walls [4,5]. Calcium ions, which are divalent, will preferentially accumulate, but also other cations are present in the double layer. As a result, positive ions are to a less degree mobile than negative ions. The charge distribution in the double layer can be assumed according to the Gouy–Chapman model [28], where the positive charge required to balance the negative charge of the cement hydration products is distributed in a diffuse manner – rather than being considered as fixed in a single Helmholtz-plane – and decreases with distance from the solid surface. The potential in the double layer can be expressed as follows [28]:

$$\frac{\psi_x}{\psi_0} = e^{-\kappa x} \tag{9}$$

where x is the coordinate into the solution, ψ_x is the potential at distance x, and ψ_0 is the potential at the solid surface ($x = 0$); κ is the Debye–Hückel parameter and the inverse, $1/\kappa$, is called the Debye–Hückel-length [1,28]:

$$\kappa^{-1} = \sqrt{\frac{RT\varepsilon_0\varepsilon}{2F^2 I}} \tag{10}$$

In this equation, ε_0 is the permittivity of free space (8.85×10^{-12} C^2 J^{-1} m^{-1}), ε is the relative permittivity of the solution, I refers to ionic strength of the solution (mol m^{-3}), and R, T and F have their usual meanings in electrochemistry. Thus, the potential–distance relation in Eq. (9) depends on ionic strength of the solution. For more concentrated solutions, the potential falls more sharply and double layer effects vanish at shorter distances from the solid surface as is apparent from Fig. 13, where this was plotted for some selected ionic strengths.

In the present mortar, the degree of capillary saturation stabilised around 80–90% (Fig. 5), which corresponds to a relative humidity (RH) in the range 92–98% [29]. From capillary condensation theory (Kelvin–Laplace equation, e.g. Ref. [30]) the stable radius of capillaries can for these RH values be estimated at 13–54 nm. Fig. 13 shows that for ionic strengths of common pore solutions, i.e. well above 0.2 mol dm^{-3}, double layer effects essentially vanish at a distance of 1–2 nm from the pore walls. This implies that in the present case, the major part of solution in capillary pores is unaffected by the electronegativity of hydrated cement. When the relative humidity decreases, however, the radius

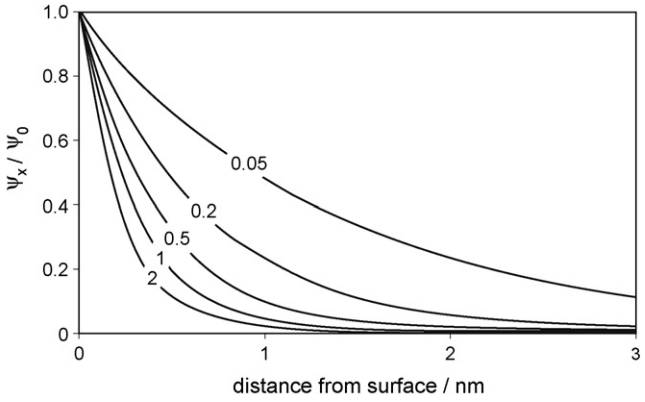

Fig. 13. Relative potential as a function of distance into the solution according to the Gouy–Chapman model, plotted for several ionic strengths (mol dm^{-3}) as indicated on the curves.

of stable menisci becomes smaller – for instance ~3 nm for RH = 70% or ~2 nm for RH = 60% – and thus the effect of the double layer becomes more pronounced. When capillary pores get discontinued, ion movement has to occur through gel pores. As the size of these interlayer spaces is commonly estimated in the range of a few nanometres, double layers of opposite pore walls can be expected to overlap, which significantly slows down ionic mobility. Permselective behaviour of cement paste can thus be expected at lower relative humidities, lower w/c ratios and possibly higher degrees of hydration, where the size of water-filled capillaries gets smaller or when discontinuous capillary porosity forces the charge to be transported through the bottlenecks of interlinking gel pores. This is schematically depicted in Fig. 14. The effect of w/c ratio on diffusivity of cations and anions has been confirmed experimentally for fully saturated specimens [3]. In addition, Tuuttis [7] data suggests that also the ratio D_{OH^-}/D_{Cl^-} deviates from bulk solution behaviour for a lower w/c ratio (Table 1).

In the present case, it appears that complete capillary discontinuity has not been reached. Fig. 4 shows that the electric resistance between the stainless steel tubes increases almost linearly with

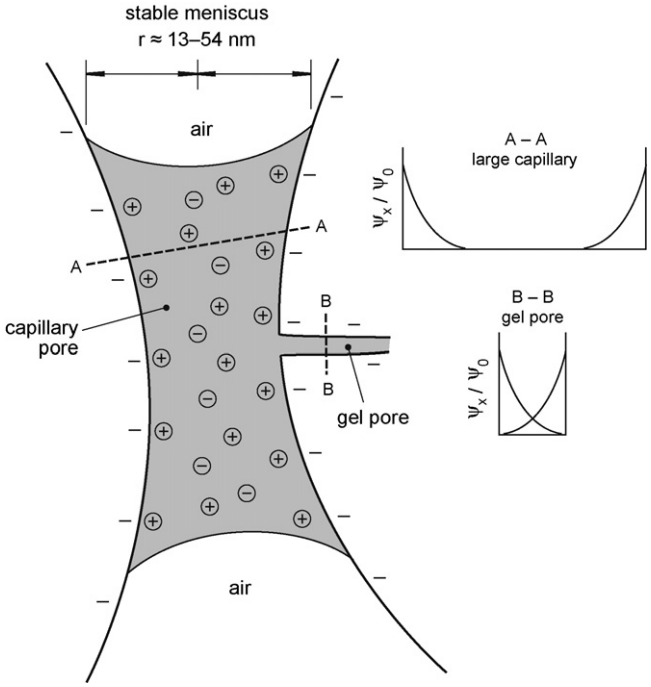

Fig. 14. Schematic illustration of pore size and double layer effects.

time (even though pore solution composition and degree of hydration have achieved stable values (Figs. 2 and 3)). The resistivity of concrete is mainly determined by ionic conductivity of the pore solution, amount of water present in the pores, tortuosity of the current pathways, and temperature (constant in the present case) [24,31–34]. The effect of ionic conductivity is apparent from Fig. 4, since the resistivity is clearly lower in layer II and III, where both hydroxide and chloride concentrations are higher. The solution conductivity, however, can be assumed to be more or less constant over time after 15 d (Fig. 3). The degree of capillary saturation stabilises at a value above 80% (Fig. 5). According to Østvik [32], the resistivity of mature Portland cement concrete with w/c = 0.6 changes only slightly with moisture content as long as DCS > 40%, namely ca. 30 Ωm per percent of DCS. When completely ascribing the observed increase in resistivity after ca. 15 d shown in Fig. 4 to a change in moisture content, this would correspond to a decrease in DCS by less than 1%. As a matter of fact, the internal moisture state (Fig. 5) does not exhibit significant changes after 2 weeks owing to the slow rate of hydration (self-desiccation). It is thus likely, that it is the microstructure, which dominates the resistivity at this stage. The proceeding hydration increases the tortuosity of the current paths by gradually blocking and narrowing capillary pores. According to Powers et al. [35], capillary continuity is lost at around 92% degree of hydration in the case of w/c = 0.6. In contrast, other researchers did not observe depercolation in cement pastes with w/c = 0.6 at all, as discussed in Ref. [36]. According to Fig. 2, the estimated degree of hydration approaches 90% by 28 d. It is reasonable to assume that the electric resistivity increases if part of the current pathways, most of them leading through continuous capillary pores, is not available anymore. As long as there is no tendency for the resistivity to level out, however, there might still be a considerable amount of large unconstricted capillaries. Thus, ionic transport processes, that is current flow, can process without being forced through interlayer spaces and gel pores.

5.2. Relative importance of liquid junction and membrane potentials

It was experimentally confirmed that the composition of the wetting electrolyte has an influence on the observed potential. Even when using highly alkaline solutions such as 0.35 M KOH, which is similar in composition to the actual pore solution, liquid junction potential errors in the range of 2–4 mV arise (Fig. 7). The strong sensitivity to even small pH differences can be explained by the markedly higher mobility of hydroxide ions compared with any other ion (Table 1). Gradients in pH are also the main factor determining the magnitude of diffusion potentials inside the concrete. Whereas pure chloride concentration gradients are of minor importance as long as the pH is high, Fig. 9 shows that in the present case, internal diffusion potentials are up to 8 mV for differences in hydroxide concentration as small as 0.15 mol dm^{-3}. The magnitude of this potential drop is expected to increase for lower w/c ratios or moisture contents, where larger fractions of the pore solution become affected by double layer effects, as well as for generally lower pH values as for instance in the case of pozzolanic additions or carbonated concrete.

For most potential measurements performed in connection with reinforced concrete, this is not critical. In the case of application of ISE, on the other hand, a measurement error of already a few millivolts adversely affects the accuracy of the chloride measurement technique [14,15]. These errors have thus to be taken into account when applying direct potentiometry to cement based materials. For instance, measurement vs. an external reference electrode across a carbonated cover zone would induce dramatic errors. Membrane behaviour of hardened cement paste also affects ionic transport. It was shown in connection with the results plotted in Fig. 11 that

under certain circumstances, an electric field is established that might force certain ions to move in the opposite direction of what is expected when solely considering their concentration profile. The transport of a certain species is always dependent on characteristics and abundance of other ions. This has to be born in mind when evaluating data from diffusion cell experiments, where often one single species is considered. More knowledge about diffusion potentials and membrane characteristics is needed for denser concrete and lower pH levels (lower w/c ratios, alternative cement types). It is also important to recognise that it is the unsaturated state that often is the relevant one; the significance of data acquired from saturated samples is questionable.

6. Conclusions

An experimental setup based on the use of embedded ion selective electrodes has proven to be suitable for the measurement of membrane potentials in mortar. Drawbacks inherent to diffusion cell based arrangements can be avoided; for instance, the present setup allows studying diffusion potentials in a moisture state below saturation.

Both liquid junction and membrane potentials have to be considered as error sources for the application of direct potentiometry in cement based materials. While the first can be kept small by the use of suitable wetting electrolytes, the latter are determined by concentration gradients within the concrete, the general level of pH, as well as permselective characteristics of the cement paste. The magnitude of concentration differences in the measurement circuit can be influenced by carefully selecting the position of the reference electrode. Potential wells offer a good possibility to avoid large gradients in pH or chloride concentration in the cover zone.

Porous Portland cement mortar with w/c = 0.6 did not show significant permselective behaviour – even not after reaching a stable moisture state by self-desiccation (80–90% DCS), which often is the relevant state for practice. Theoretical considerations and experimental data suggest that the stable radius of water-filled capillaries is in this state still large enough to allow ionic transport through those fractions of pore solution that are unaffected by double layer effects. In the studied case, internal diffusion potentials reached up to 8 mV given the presence of pronounced chloride and moderate pH gradients. It is expected that the magnitude increases at lower pH, lower moisture content, as well as lower w/c ratios, but this has yet to be validated and quantified by further research.

Acknowledgement

The work described in this paper forms part of the Norwegian COIN project (www.sintef.no/coin).

References

[1] V.S. Bagotsky, Fundamentals of Electrochemistry, 2nd ed., John Wiley & Sons, 2006, The Electrochemical Society Series.
[2] S. Goto, D.M. Roy, Cem. Concr. Res. 11 (1981) 751.
[3] A. Atkinson, A.K. Nickerson, J. Mater. Sci. 19 (1984) 3068.
[4] S. Chatterji, M. Kawamura, Cem. Concr. Res. 22 (1992) 774.
[5] S. Chatterji, Cem. Concr. Res. 24 (1994) 1229.
[6] Y. Elakneswaran, T. Nawa, K. Kurumisawa, Mater. Struct. 42 (2009) 83.
[7] K. Tuutti, Corrosion of Steel in Concrete, Swedish Cement and Concrete Research Institute, 1982.
[8] Handbook of Chemistry and Physics, 90th ed., CRC-Press, 2009–2010.
[9] L. Tang, Cem. Concr. Res. 29 (1999) 1463.
[10] J.-Z. Zhang, N.R. Buenfeld, Cem. Concr. Res. 27 (1997) 853.
[11] J.-Z. Zhang, N.R. Buenfeld, Mater. Struct. 33 (2000) 492.
[12] J.-Z. Zhang, J.Y. Li, N.R. Buenfeld, Cem. Concr. Comp. 24 (2002) 451.
[13] U. Angst, Ø. Vennesland, R. Myrdal, Mater. Struct. 42 (2009) 365.
[14] U. Angst, Ø. Vennesland, Mater. Corros. 60 (2009) 638.
[15] U. Angst, B. Elsener, C.K. Larsen, Ø. Vennesland, J. Appl. Electrochem. 40 (2010) 561.
[16] E. Samson, J. Marchand, Comput. Struct. 85 (2007) 1740.
[17] B. Elsener, L. Zimmermann, H. Böhni, Mater. Corros. 54 (2003) 440.
[18] COMSOL Multiphysics V3.5a.
[19] C.K. Larsen, Chloride binding in concrete, Dr. Ing. Thesis, Report No. 1998:101, Norwegian University of Science and Technology, 1998.
[20] E.J. Sellevold, H. Justnes, 4th International Conference on Fly Ash, Silica Fume, Slag, and Natural Pozzolans in Concrete, CANMET/ACI, Istanbul, Turkey, 1992, p. 891.
[21] T.C. Powers, T.L. Brownyard, Studies of the Physical Properties of Hardened Portland Cement Paste, Research Laboratories of the Portland Cement Association, Bulletin 22, 1948.
[22] T.C. Powers, Proceedings of the 4th International Symposium on Chemistry of Cement, Washington, DC, 1960, p. 577.
[23] H. Justnes, Nordic Concrete Research, Nordic Concrete Federation, Norsk Betongforening, Oslo, 1998, p. 48 (Publication No. 21. 1/98).
[24] D.A. Whiting, M.A. Nagi, Electrical Resistivity of Concrete—A Literature Review, Portland Cement Association, Skokie, IL, 2003.
[25] R.K. Dhir, M.R. Jones, H.E.H. Ahmed, Cem. Concr. Res. 20 (1990) 579.
[26] J. Marchand, Mater. Struct. 34 (2001) 195.
[27] S.W. Yu, G. Sergi, C.L. Page, Mag. Concr. Res. 45 (1993) 257.
[28] J.O.M. Bockris, A.K.N. Reddy, M. Gamboa-Aldeco, Modern Electrochemistry, vol. 2A: Fundamentals of Electrodics, 2nd ed., Kluwer Academic/Plenum Publishers, 2000.
[29] R.H. Relling, E.J. Sellevold, Proceedings of the International Conference on Concrete Repair Rehabilitation and Retrofitting, Cape Town, South Africa, Taylor & Francis/Balkema, The Netherlands, 2006, p. 191.
[30] Z.C. Grasley, D.A. Lange, Mater. Struct. 40 (2007) 311.
[31] F. Hunkeler, Constr. Build. Mater. 10 (1996) 381.
[32] J.-M. Østvik, Thermal aspects of corrosion of steel in concrete, Doctoral thesis 2005:5, Norwegian University of Science and Technology, 2005.
[33] R. Polder, C. Andrade, B. Elsener, Ø. Vennesland, J. Gulikers, R. Weidert, M. Raupach, Mater. Struct. 33 (2000) 603.
[34] D. Bürchler, B. Elsener, H. Böhni, Electrically based microstructural characterization, in: R.A. Gerhardt, S.R. Taylor, E.J. Garboczi (Eds.), Mat. Res. Soc. Symp. Proc., vol. 411, 1996, p. 407.
[35] T.C. Powers, L.E. Copeland, H.M. Mann, Capillary continuity or discontinuity in cement pastes, J. PCA Res. Dev. Lab. (May) (1959) 38.
[36] G. Ye, Cem. Concr. Res. 35 (2005) 167.